Faculty Publications

2005-06-01

The Effect of Oxygen on Nonthermal-Plasma Reactions of Nitrogen Oxides in Nitrogen

Morris D. Argyle
mdargyle@byu.edu

Gui-Bing Zhao

S.V.B. Janardhan Garikipati

Xudong Hu

Maciej Radosz

Original Publication Citation

BYU ScholarsArchive Citation

The Effect of Oxygen on Nonthermal-Plasma Reactions of Nitrogen Oxides in Nitrogen

Gui-Bing Zhao, S.V.B.Janardhan Garikipati, Xudong Hu, Morris D. Argyle, Maciej Radosz[*]
Department of Chemical & Petroleum Engineering, University of Wyoming, Laramie, WY 82071-3295, USA

Abstract

NO is mainly converted to NO_2 by chemical oxidation in the presence of oxygen. Initial selectivity analysis shows that three electron collision reactions are important for NO_x evolution in O_2/N_2. The rate constants of these reactions decrease with increasing oxygen concentration. This is because oxygen is electronegative and hence reduces electron concentration. The rate constant of O_2 dissociation by electron collision reaction is almost two orders of magnitude higher than that of N_2 dissociation. NO formation occurs predominantly through $N(^2D) + O_2 \rightarrow NO + O$. The critical oxygen concentration, defined as the concentration above which the NO_x formation rate exceeds the NO_x decomposition rate, increases with increasing the initial NO concentration.

Submitted to *AIChE J*

---

[*] Corresponding author. E-mail: radosz@uwyo.edu, tel: 307-766-2500, fax: 307-766-6777

Introduction

The removal of nitrogen oxides (NO_x) from combustion exhaust streams has become an important international technology issue because of the key role NO_x play in many global environmental problems, such as acid rain, photochemical smog formation, and the greenhouse effect. There is considerable political pressure for the adoption of increasingly stringent emission standards. Among the emerging technologies for NO_x decomposition, non-thermal plasma is one of the most promising. A pulsed corona discharge reactor (PCDR) is one of the non-thermal plasma technologies characterized by low gas temperature and high electron temperature achieved by producing high energy electrons in the gas while leaving the bulk temperature of the gas unchanged. A PCDR utilizes a high-voltage short-duration (<100 ns) electrical discharge between non-uniform electrodes to produce streamers through the growth of electron avalanches formed by electron collision ionization events in the gas.[1] A streamer is a region of highly ionized gas in which a variety of active radicals and chemical species are formed through electron collision reactions with the background gas.[2] These active species, in turn, initiate bulk phase reactions that lead to NO_x conversion.

NO_x removal is generally a problem of NO removal because NO accounts for about 95 mol% of NO_x emitted.[3] There are two main pathways for NO conversion: chemical oxidation and chemical reduction. Conversion of NO to its molecular elements (N_2 and O_2) through chemical reduction is one of the most attractive methods, especially for mobile source applications.

NO conversion in N_2 using non-thermal plasma has been extensively investigated.[2, 4-8] In such a system, NO is readily converted to benign gas (N_2 and O_2) through a reduction mechanism involving N radicals, with formation of only small amounts of byproduct N_2O (1-2% of initial NO concentration).[9] However, real combustion flue gas, for example, from furnaces

and fired heaters, contains 1-6% of oxygen depending on combustion conditions.[10] Our recent measurements indicate the oxygen concentration in diesel engine exhaust is even higher (12~14%), which makes NO conversion more complex.

Oxygen can reduce the rate of NO reduction to N_2 and O_2 in two ways. First, as an electronegative gas (with an electron affinity of 0.45 eV for O_2 compared to about -1.5 eV for N_2),[11, 12] oxygen decreases the discharge current due to the electron attachment process, as found by Kanazawa *et al.*[13] and Mok *et al.*[14] Sathiamoorthy *et al.*[2] investigated the NO_x reaction mechanism in nitrogen and dry air by both experiment and simulation. They found that the electron density in dry air decreases by several orders of magnitude compared to that in N_2 due to the effect of the electron attachment to O_2. A similar effect of oxygen on the electrical discharge was observed by Gallimberti.[15] Therefore, the presence of oxygen decreases the formation rate of N radicals, which decreases the NO reduction rate to benign N_2 and O_2. Second, oxygen has a lower dissociation energy (5.2 eV/molecule) than nitrogen (9.8 eV/molecule[16]), which causes electrons to preferentially interact with O_2 to produce strongly oxidizing species such as O and O_3. These oxidizing species promote the oxidation of NO to produce byproducts, such as NO_2 and N_2O, instead of the desired reduction products, N_2 and O_2. McLarnon and Penetrante[17] investigated the effect of 0-6% oxygen concentrations on NO_x conversion and found that the amount of NO chemically reduced to N_2 decreases and the amount of NO oxidized to NO_2 increases, as the O_2 content increases. Tas *et al.*[18] carried out detailed studies on the effect of O_2 on energy consumption and NO removal efficiency in N_2. They found that over 90% of NO conversion occurs through oxidation in the presence of O_2. Therefore, total NO_x (NO, NO_2 and N_2O) conversion in the corona discharge remarkably declines in oxygen-rich gases, such as $N_2/O_2/NO$ gas mixtures.[2, 8, 19, 20] As a result of the relative ease of dissociating O_2,

under certain conditions, NO_x conversion becomes negative in the presence of O_2 (i.e., NO_x is produced). Yan et al.[8] found that the rate of oxidation reactions exceeds the rate of reduction reactions, such as $N + NO \rightarrow N_2 + O$, when the O_2 concentration is higher than 3.6%. Penetrante et al.[21] found that the reduction of NO with ground state N atoms is almost completely counterbalanced by the production of NO at 10% O_2 concentration. Finally, Aritoshi et al.[20] found that the production of NO_x becomes dominant when the concentration of O_2 reaches 2%. These literature results show that there is a critical oxygen concentration above which the NO_x formation rate exceeds the NO_x decomposition rate.

However, some issues are still unclear. The first is the mechanism of NO formation during electrical discharge in the presence of O_2. Gentile and Kushner[22, 23] investigated microstreamer dynamics during plasma remediation of NO using atmospheric pressure dielectric barrier discharges. They reported that NO formation occurs through reaction with ground state N radicals, $N(^4S)$, by the reaction $N(^4S) + O_2 \rightarrow NO + O$ because local energy deposition in the streamers can produce high temperatures that initiate advection and facilitate production of NO. Kim et al.,[24] Lowke and Morrow[25] and Mukkavilli et al.[26] proposed a similar mechanism of NO formation. However, Aritoshi et al.[20] proposed that excited N radicals, $N(^2D)$, are the primary species responsible for NO formation, through the reaction $N(^2D) + O_2 \rightarrow NO + O$. Herron,[7] Yan et al.,[8] Penetrante et al.,[21] and Orlandini and Riedel[27] presented similar mechanisms for NO formation. Second, the formation and conversion of byproducts are rarely reported and explained, especially for N_2O. Third, the relationship between the rate of electron collision reactions and oxygen content and the selectivity of electron collision reactions for the dissociation of N_2 and O_2 are rarely reported. Finally, the critical oxygen content may change

with the initial NO concentration, but no detailed studies on the critical oxygen content have been reported.

Therefore, the goals of this work are to study the effect of O_2 on NO conversion in a PCDR, through experiments and simulation, to clarify the mechanism of NO_x formation and conversion in the presence of O_2, to understand the relationship between the rate of electron collision reactions and oxygen content, and to study the relationship between the critical oxygen content and initial NO concentration.

Experimental

The experimental setup is shown in Figure 1. The test gas was prepared by mixing the gas from the two sets of gas cylinders, one set with NO in N_2 (three concentrations were used: 655 ppm NO, 659 ppm NO, or 800 ppm NO in ultra high purity N_2, US Airgas) and the other set with O_2 in N_2 (four concentrations were used, approximately: 5% O_2, 10% O_2, 15% O_2 and 30% O_2 in ultra high purity N_2, USAirgas). These gases were mixed through a careful flow rate control to obtain the desired concentrations of NO and O_2 in nitrogen fed to PCDR shown in Table 1. The PCDR feed was prepared and maintained at ambient temperature (~300 K). The pressure in the PCDR was maintained at 217 kPa with control valves on the outlet gas lines. The oxygen concentration at the PCDR outlet was analyzed using a Hewlett Packard 5890 series II Gas Chromatograph (GC) with a thermal conductivity detector (TCD) and an Alltech CTR I column (outer tube with 6 ft × 1/4″ packing of activated molecular sieve and inner tube with 6 ft × 1/8″ packing of porous polymer mixture). The outlet gas was collected in 300 ml stainless steel cylinders (as shown in Figure 1) and analyzed for stable nitrogen oxides using a Spectrum 2000 Perkin-Elmer Fourier transform infrared spectrometer (FTIR) with a narrow-band mercury cadmium telluride (MCT) detector.

The PCDR used in this work consisted of a high-voltage power supply with control unit and pulser/reactor assembly, as explained previously in detail.[28] The high voltage controller contained electronic and gas controls required to regulate the high voltage charging power supply as well as the pulsed power delivered to the reactor gas. The pulser/reactor assembly contained the pulsed power generator and the pulsed corona discharge reaction chambers. The reactor had ten parallel reaction tubes, each 914 mm in length and 23 mm in diameter, with a stainless steel wire, 0.58 mm in diameter, passing axially through the center of each tube. The wire was positively charged and the tube was grounded. The gas flowing through the reactor tube was converted to a plasma by high voltage discharge from the reactor anodes. One tube was fitted with UV-grade quartz windows for diagnostics and plasma observation. The energy delivered to the reactor per pulse can be calculated either from time integral of the product of the measured pulse discharge voltage (V) and current (I) or from $(1/2)CV_c^2$, where C is the pulse forming capacitance, 800 pF; V_c is the constant charge voltage, 19.2 ± 1 kV, in the pulse forming capacitance before discharge. The discrepancy between the calculated values for energy per pulse using these two methods is measured to be less than 3%. Since the current can fluctuate and be shifted in phase relative to voltage, and since the delay times of the voltage sensor and current sensor cannot be measured accurately, the second method should be more reliable. Therefore, the second method, $(1/2)CV_c^2$, is used to calculate energy input per pulse in this work. The power consumed, W ($J \cdot s^{-1}$), is calculated as the product of the input energy per pulse and the pulse frequency. The specific energy input, Es ($kJ \cdot m^{-3}$), is defined as

$$Es = \frac{W}{1000 \cdot u} \tag{1}$$

where u is gas flowrate ($m^3 \cdot s^{-1}$). The system design permitted variation and measurement of the applied voltage and frequency and of the reactor current and voltage.

The plasma reactor described above was modeled using a lumped kinetic model that describes the evolution of all species, reported elsewhere.[5]

Results and Discussion

Experimental observations

Figure 2 shows the FTIR spectra for NO conversion in N_2 (Figure 2(a)) and in 4.60% O_2 in N_2 (Figure 2(b)) at a pulse frequency of 200 Hz and applied voltage of ~20 kV. Similar FTIR spectra were obtained during NO conversion with the other oxygen concentrations shown in Table 1. Only NO, NO_2 and N_2O were detected in these spectra of the outlet gas from the PCDR. Other nitrogen oxides, such as N_2O_5 (peaks expected at 787.90-793.89 cm^{-1} and 1217.09-1305.73 cm^{-1}),[29] and O_3 (peaks expected at 980-1080 cm^{-1})[29] were not detected. The FTIR detection limit is 5 ppm for both nitrogen oxides and ozone. Herron[7] simulated the NO reaction in dry air and found that N_2O_5 should be formed as a terminal product, but no experimental data support this conclusion.

Figures 3(a), (b) and (c) show the evolution of NO, NO_2 and N_2O concentrations, respectively, as functions of specific energy inputs. In the absence of O_2, the NO concentration decreases quickly to zero with increasing specific energy input (filled squares in Figure 3(a)). The NO_2 concentration initially increases to a maximum with increasing specific energy input, and then decreases to zero at the same specific energy input at which the NO concentration reaches zero (filled squares in Figure 3(b)). The N_2O concentration also increases to a maximum and then decreases to a constant value with increasing specific energy input (filled squares in Figure 3(c)). Figure 3(d) shows the NO_x conversion as a function of specific energy input. The NO_x conversion can be defined as the fraction of NO converted to N_2, expressed as follows:

$$X_{NO_x} = \frac{C_{i,NO} - C_{o,NO} - C_{o,NO_2} - 2 \times C_{o,N_2O}}{C_{i,NO}} \times 100\% \qquad (2)$$

where C_i is the concentration of a given species at the reactor inlet (ppm) and C_o is the concentration of a given species at the reactor outlet (ppm). In the absence of O_2, the overall NO_x conversion initially increases linearly with increasing specific energy input until reaching a constant value at $98.5 \pm 0.5\%$ because of the difficulty of converting N_2O (filled squares).[4, 5, 9] This behavior of NO_x concentrations in pure N_2 can be explained quantitatively using the reaction mechanism developed previously.[4, 5, 9]

However, when oxygen is present, the NO conversion and byproduct formation is more complex. At low O_2 concentrations, for example 2.28% O_2 (open circles in Figure 3(a)), the NO concentration decreases quickly with increasing specific energy input for low specific energies (<100 kJ/m^3), but at high specific energy input (>100 kJ/m^3), it decreases slowly with increasing specific energy input. NO is not fully converted at the highest specific energy tested. At high O_2 concentrations ($\geq 4.60\%$ O_2, open triangles in Figure 3(a)), the NO concentration initially decreases with increasing specific energy input until it reaches a minimum, after which it increases slowly with increasing specific energy input. Figure 3(b) shows that the NO_2 concentration forms a shallow maximum at the two lower oxygen concentrations, while it increases continually with increasing specific energy at the two higher oxygen concentrations. NO_2 cannot be completely converted in the presence of O_2 at the same specific energy inputs at which NO_2 is completely converted in the absence of O_2. In contrast to N_2O in the absence of oxygen, Figure 3(c) shows that there is no maximum for N_2O formation in the presence of oxygen. The N_2O concentration increases continuously with increasing specific energy input. At a given specific energy input, the amount of NO_2 and N_2O formed increases with increasing oxygen content, as shown in Figures 3(b) and (c), respectively. The NO_x conversion shown in
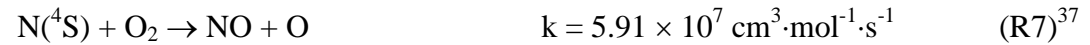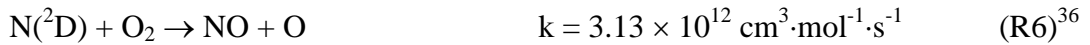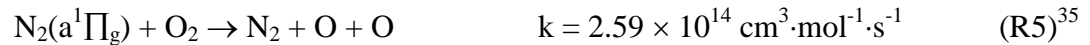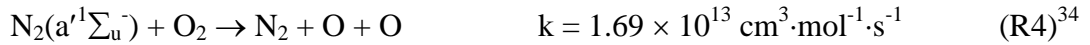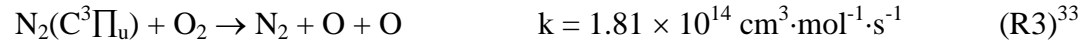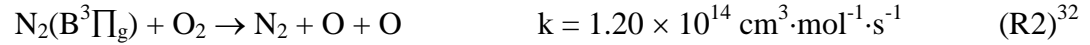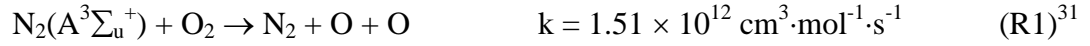
Figure 3(d) changes from a positive value to a negative value for all oxygen concentrations greater than ~2.5%. According to Eq. (2), a positive NO_x conversion means that some NO is converted to N_2 and O_2. However, a negative NO_x conversion means that the amount of NO_x formed is greater than the amount of NO reduced to N_2/O_2. The amount of NO_x formed increases with increasing oxygen concentration. This phenomenon will be further discussed in terms of the lumped model.[5]

Electron Collision Reactions

The collisions of energetic electrons produced by the electrical discharge with gas molecules produce chemically active species, such as radicals and ions, which contribute to NO_x formation and conversion.[30] The initial selectivity analysis developed recently[4] was used to identify the chemically active species produced by electron collision reactions that are important in NO_x formation and conversion. For this analysis, electron interactions with species other than N_2 and O_2 were not considered since their concentrations relative to N_2 and O_2 are always very low.[5, 30] Further, McLarnon and Penetrante[17] found that charged species do not contribute significantly to NO_x conversion. Our previous investigation[4] on NO_x conversion in non-thermal nitrogen plasma confirmed that cations, such as N_2^+, do not contribute to NO_x conversion. Therefore, reactions with ions are not considered in this analysis.

As reported recently,[4] the possible chemically active species formed from electron collision reactions with nitrogen include $N_2(A^3\Sigma_u^+)$, $N_2(B^3\Pi_g)$, $N_2(B'^3\Sigma_u^-)$, $N_2(a'^1\Sigma_u^-)$, $N_2(a^1\Pi_g)$, $N_2(W^1\Delta_u)$, $N_2(C^3\Pi_u)$, $N_2(E^3\Sigma_g^+)$, $N(^4S)$, and $N(^2D)$. An initial selectivity analysis of systematic experiments performed in absence of O_2 showed that the active species which play an important role in NO_x conversion are $N_2(A^3\Sigma_u^+)$ and $N(^4S)$.[4] Other active species are mainly quenched to the ground state by the nitrogen background gas. However, at percent-level O_2 concentrations,

the situation may be different because these active species contribute to O_2 dissociation or NO_x formation by the following reactions (at 300 K):

$$N_2(A^3\Sigma_u^+) + O_2 \rightarrow N_2 + O + O \qquad k = 1.51 \times 10^{12} \text{ cm}^3 \cdot \text{mol}^{-1} \cdot \text{s}^{-1} \qquad (R1)^{31}$$

$$N_2(B^3\Pi_g) + O_2 \rightarrow N_2 + O + O \qquad k = 1.20 \times 10^{14} \text{ cm}^3 \cdot \text{mol}^{-1} \cdot \text{s}^{-1} \qquad (R2)^{32}$$

$$N_2(C^3\Pi_u) + O_2 \rightarrow N_2 + O + O \qquad k = 1.81 \times 10^{14} \text{ cm}^3 \cdot \text{mol}^{-1} \cdot \text{s}^{-1} \qquad (R3)^{33}$$

$$N_2(a'^1\Sigma_u^-) + O_2 \rightarrow N_2 + O + O \qquad k = 1.69 \times 10^{13} \text{ cm}^3 \cdot \text{mol}^{-1} \cdot \text{s}^{-1} \qquad (R4)^{34}$$

$$N_2(a^1\Pi_g) + O_2 \rightarrow N_2 + O + O \qquad k = 2.59 \times 10^{14} \text{ cm}^3 \cdot \text{mol}^{-1} \cdot \text{s}^{-1} \qquad (R5)^{35}$$

$$N(^2D) + O_2 \rightarrow NO + O \qquad k = 3.13 \times 10^{12} \text{ cm}^3 \cdot \text{mol}^{-1} \cdot \text{s}^{-1} \qquad (R6)^{36}$$

$$N(^4S) + O_2 \rightarrow NO + O \qquad k = 5.91 \times 10^{7} \text{ cm}^3 \cdot \text{mol}^{-1} \cdot \text{s}^{-1} \qquad (R7)^{37}$$

Therefore, the chemically active species produced by electron collision reactions with nitrogen may be consumed by four parallel processes:

(1) Natural radiation accompanying optical emission:

$$A^* \rightarrow A + h\nu \qquad\qquad R_I = k_I \cdot C_{A^*}$$

(2) Quenching with the background gas N_2:

$$A^* + N_2 \rightarrow A + N_2 \qquad\qquad R_q = k_q \cdot C_{A^*} \cdot C_{N2}$$

(3) Dissociative quenching or reaction with background gas O_2:

$$A^* + O_2 \rightarrow \text{products} \qquad\qquad R_d = k_d \cdot C_{A^*} \cdot C_{O2}$$

(4) Reaction with NO_x (conversion of NO_x):

$$A^* + NO_x \rightarrow \text{products} \qquad\qquad R_r = k_r \cdot C_{A^*} \cdot C_{NOx}$$
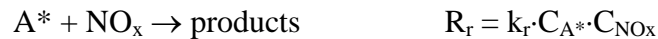
In these chemical equations, A^* represents any active species; k_I, k_q, k_d and k_r are the rate constants of radiation, quenching, dissociative quenching of O_2, and NO_x conversion, respectively; and R_i is the reaction rate of reaction type i. The initial selectivity of these four parallel processes can be defined as

$$S_I = \frac{R_I}{R_I + R_q + R_d + R_r} = \frac{k_I}{k_I + k_q C_{N_2} + k_d C_{O_2} + k_r C_{NOx}} \times 100\% \tag{3a}$$

$$S_q = \frac{R_q}{R_I + R_q + R_d + R_r} = \frac{k_q C_{N_2}}{k_I + k_q C_{N_2} + k_d C_{O_2} + k_r C_{NOx}} \times 100\% \tag{3b}$$

$$S_d = \frac{R_d}{R_I + R_q + R_d + R_r} = \frac{k_d C_{O_2}}{k_I + k_q C_{N_2} + k_d C_{O_2} + k_r C_{NOx}} \times 100\% \tag{3c}$$

$$S_r = \frac{R_r}{R_I + R_q + R_d + R_r} = \frac{k_r C_{NOx}}{k_I + k_q C_{N_2} + k_d C_{O_2} + k_r C_{NOx}} \times 100\% \tag{3d}$$

where S_I, S_q, S_d and S_r are the initial selectivities to radiative emission reactions, quenching reactions, O_2 dissociation, and NO_x conversion reactions, respectively.

The analysis of initial selectivity is an effective method to examine the significance of the active species. Only the active species which contribute predominantly to NO_x formation and conversion need to be considered. In this work, the highest NO_x concentration in the presence of O_2 is less than 600 ppm, while the lowest O_2 concentration is 2.28% (mol/mol) in the N_2 balance gas. At 217 kPa and 300K, these concentrations of NO_x, O_2 and N_2 are 5.21×10^{-8} mol/cm^3, 1.98×10^{-6} mol/cm^3, and 8.49×10^{-5} mol/cm^3, respectively. Substituting these concentrations and the rate constants for consumption of active species (A*) by radiation, quenching, dissociative quenching of O_2, and NO_x conversion (summarized in our previous work[4]) in equations 3a through 3d, yields the initial selectivities for the four parallel processes presented in Table 2. These results indicate that all of the electronic excited states of molecular nitrogen contribute predominantly to O_2 dissociation or quenching. Moreover, with increasing O_2 concentration, the contribution of these active species to O_2 dissociation further increases.

Therefore, only N(^{2}D), which is an excited atomic N radical, and N(^{4}S), which is the ground state atomic N radical, may directly contribute to NO formation through reactions R6 and

R7. However, a simple comparison shows that $N(^4S)$ cannot contribute significantly to NO formation regardless of the $N(^4S)$ concentration. Under the most conservative circumstance of low NO concentration (e.g. 50 ppm NO in the presence of O_2 in the reactor, shown in Figure 3(a)), the rate of NO formation by R7 is about 500 times lower than the rate of NO decomposition by reaction $N(^4S) + NO \rightarrow N_2 + O$, which has a rate constant of 1.87×10^{13} $cm^3 \cdot mol^{-1} \cdot s^{-1}$.[38] Therefore, $N(^4S)$ atoms are mainly consumed in reactions with NO and NO_2. As a result, the mechanism of NO formation is predominantly through $N(^2D)$ in R6. With increasing oxygen concentration, the selectivity of NO formation through $N(^2D)$ further increases. Cosby[39] found that the dominant dissociation mechanism in pure N_2 plasmas is $N_2 \rightarrow N(^2D) + N(^4S)$, indicating that approximately equal amounts of $N(^2D)$ and $N(^4S)$ are formed. Hill *et al.*[40] found that the yield of $N(^2D)$ during N_2 dissociation in air corona discharges is ~67%, which means that $N(^2D)$ is formed at twice the rate of $N(^4S)$. Both of these results are consistent with the proposal that NO formation occurs through reaction with $N(^2D)$ in R6, but they do not provide a consistent value for the relative proportions of $N(^2D)$ and $N(^4S)$.

Similar to electron collisions with nitrogen, many active species may be produced when electrons collide with molecular oxygen. Again, the active oxygen species that actually contribute to NO_x formation and conversion must be determined. The potential energy curve of molecular and atomic oxygen is reported in reference 41. Only two electronic states of O atoms [$O(^3P)$ and $O(^1D)$] are energetically accessible at the experimental conditions of this study because the average electron energy in the PCDR is less than 10 eV,[42, 43] as supported by investigation of Eliasson and Kogelschatz.[44] $O(^3P)$ and $O(^1D)$ are the ground state and the first electronic excited state of atomic O radicals, respectively. Therefore, the possible chemically active species formed from electron collision reactions with oxygen are $O_2(a^1\Delta_g)$, $O_2(b^1\Sigma_g^+)$,

$O_2(c^1\Sigma_u^-)$, $O_2(C^3\Delta_u)$, $O_2(A^3\Sigma_u^+)$, $O_2(^3\Pi_u)$, $O_2(^1\Pi_u)$, $O_2(^3\Sigma_g^-)$, $O_2(B^3\Sigma_u^-)$, $O_2(^1\Pi_g)$, $O_2(^1\Delta_u)$, $O_2(^1\Delta_g)$, $O(^3P)$, and $O(^1D)$, which can be consumed by natural radiation, reaction, quenching with N_2, O_2, or NO_x.

Table 3 lists these possible interactions. Extensive literature reviews[45, 46] reported no reactions with or quenching by the following molecular O_2 electronic excited states: $O_2(^3\Pi_u)$, $O_2(^1\Pi_u)$, $O_2(^3\Sigma_g^-)$, $O_2(^1\Pi_g)$, $O_2(^1\Delta_u)$ and $O_2(^1\Delta_g)$. The data in Table 3 show that $O_2(a^1\Delta_g)$, $O_2(b^1\Sigma_g^+)$, $O_2(c^1\Sigma_u^-)$, $O_2(C^3\Delta_u)$ and $O_2(A^3\Sigma_u^+)$ are mainly quenched to the ground state, while $O_2(B^3\Sigma_u^-)$ mainly returns to the ground state through radiative emission because of the short radiative lifetime of about 40 ns.[47] Therefore, the excited states of molecular oxygen are essentially unreactive, which supports the conjecture of Herron.[7]

As a result, only $O(^1D)$ or $O(^3P)$ or both are involved in the NO_x formation mechanism. The rate constants for the quenching reactions of $O(^1D)$ by N_2 and O_2 (R31 and R32) are equal to or up to four times lower than the rate constants for the reactions of $O(^1D)$ and NO_x (R33-R36), while the total concentration of N_2 and O_2 is 167 times higher than that of NO_x (based on 600 ppm NO_x). Comparison of the reaction rates of R31-32 with those of R33-36 shows that $O(^1D)$ would be quenched by the background nitrogen and oxygen because the total reaction rate of R31-32 is at least 40 times higher than R33-36 at the prevailing reactant concentrations and any assumed $O(^1D)$ concentration. Therefore, only ground state O atoms, $O(^3P)$, contribute to NO_x evolution among all of the active species produced from electron collision reactions with molecular oxygen.

Mechanism and kinetics

The previous discussion on electron collision reactions with oxygen indicates that, although many electron collision reactions with O_2 occur in the PCDR, only the O_2 dissociation

reaction must be considered because only O atoms contribute to NO_x formation. Therefore, only the following electron collision reaction is considered for molecular O_2:

$$e + O_2 \rightarrow O(^3P) + O(^3P) + e \tag{R37}$$

As the earlier discussion on electron collision reactions with nitrogen has shown, almost all active species can contribute to NO_x evolution, either directly through formation of NO_x by $N(^2D)$ or indirectly through O_2 dissociation reactions with these excited N_2 species. Therefore, all electron collision reactions resulting in active species formation are considered:[4]

$$e + N_2 \rightarrow N(^4S) + N(^4S) + e \tag{R38}$$

$$e + N_2 \rightarrow N(^2D) + N(^2D) + e \tag{R39}$$

$$e + N_2 \rightarrow N_2(A^3\Sigma_u^+) + e \tag{R40}$$

$$e + N_2 \rightarrow N_2(B^3\Pi_g) + e \tag{R41}$$

$$e + N_2 \rightarrow N_2(B'^3\Sigma_u^-) + e \tag{R42}$$

$$e + N_2 \rightarrow N_2(a'^1\Sigma_u^-) + e \tag{R43}$$

$$e + N_2 \rightarrow N_2(a^1\Pi_g) + e \tag{R44}$$

$$e + N_2 \rightarrow N_2(W^1\Delta_u) + e \tag{R45}$$

$$e + N_2 \rightarrow N_2(C^3\Pi_u) + e \tag{R46}$$

$$e + N_2 \rightarrow N_2(E^3\Sigma_g^+) + e \tag{R47}$$

The rate constant of electron collision reactions is a function of electron energy distribution and the cross sections of electronic excitation and molecular dissociation.[26] However, the electron energy distribution in the plasma is complicated and not measurable because the electric field is strongly non-uniform, due to strong space-charge field effects, and is time dependent.[21] Further, there are large discrepancies in the reported values of the cross sections of electronic excitation

and molecular dissociation.[27] Therefore, a calculation for all of these rate constants of electron collision reactions with N_2 is not feasible.

In our kinetic model,[5] there are two parameters that describe the rate constant of each electron collision reaction, α and β, as shown in the following equation:

$$k[e] = \beta \sqrt{\frac{1}{\alpha P}} W^{0.75} \exp(-\frac{\alpha P}{W})$$ (4)

where P is the system pressure and W is the power input. This expression, based on a Maxwellian distribution function for the electron velocity, semi-empirically describes the rate of electron collision reactions through a pseudo-first order rate constant by combining the true rate constant with the electron concentration.[28] This implies that 20 model parameters would be needed to describe the ten electron collision reactions with N_2 (R38-R47), too many to produce meaningful results. However, the net effect of electron collision reactions R40-R47 is the dissociation of oxygen because all electronic excited states of molecular nitrogen predominantly contribute to O_2 dissociation or are selectively quenched, as shown in Table 2. Thus, a reasonable simplifying assumption is to model the net result of electron collision reactions R40-R47 as the single electron collision reaction R37. The contribution of all molecular nitrogen electronic excited states to O_2 dissociation is presumably far lower than that of direct electron collision reactions with O_2 because the dissociation energy per oxygen molecule, 5.2eV/O_2, is much less than the critical electronic excitation energy of all N_2 electronic excited states (Figure 1 in Reference 4).

In addition to R37, R38 and R39 (electron collision reactions that form $N(^4S)$ and $N(^2D)$, respectively) are the only electron collision reactions assumed to be important for NO_x conversion and formation in N_2/O_2 plasma. Both R38 and R39 are included due to the disagreement in previous reports on the relative amounts of $N(^4S)$ and $N(^2D)$ formed.[39, 40]

Many series and parallel reactions among active species, N_2, O_2 and NO_x are possible to follow the electron collision reactions. For example, Penetrante *et al.*[6] used 287 reactions to simulate NO_x evolution in a very simple system, NO in N_2. In the present analysis, a total of 28 reactions (shown in Table 4) were selected to simulate NO_x evolution based on a rough selectivity analysis to determine the controlling reactions by assuming that the slowest reaction among series reactions is the controlling step, while the fastest reaction among parallel reactions is the controlling step. These 28 reactions for NO_x evolution were analyzed for the $NO/N_2/O_2$ reaction system.

For such a system, six model parameters must be determined for the three electron collision reactions (R37-39) for the NO in N_2/O_2 system. There are ten components (O, N, $N(^2D)$, NO NO_2, N_2O, NO_3, O_3, O_2, N_2) in this reaction system, as shown in Table 4. Therefore, there are ten equations for each of the eight power inputs, which leads to a total of 80 equations used to determine the six parameters (α_i and β_i, i = 1-3) for a experimental system of 2.28% O_2 + 355 ppm NO in N_2 using the previously reported optimization method.[5] Figure 4 shows measured and correlated NO, NO_2, and N_2O concentrations for the experiments listed in Table 1. The correlated curves in Figure 4 represent the experimental data, which confirms that the reaction mechanism in Table 4 is a reasonable hypothesis of NO_x evolution in N_2/O_2 plasma. The concentrations of N_2 and O_2 at the outlet of the reactor used in the model calculations were obtained from nitrogen and oxygen material balances.

No O, N, O_3, NO_3, or N_2O_5 were detected at the outlet of the reactor. The absence of the atomic radicals is consistent with their reactivity, but the absence of the other three molecules was investigated using the model. The lack of ozone in the reactor effluent (Figure 2) can be explained by reaction R65. During all experimental conditions in the presence of oxygen, the NO

concentration is greater than 50 ppm (Figure 3(a)). Assuming that the NO concentration is 50 ppm (4.34×10^{-9} mol/cm^3), O_3 conversion, calculated from the rate constant for R65, is shown in Figure 5 as a function of gas residence time. O_3 can be completely converted in 0.1 s of residence time in the reactor. Therefore, NO and O_3 do not coexist in the system. By the same reasoning, NO_3 is undetectable because of reaction R66. The simulation results show that the ozone concentration is less than 1 ppm and the NO_3 concentration is less than 0.001 ppm for all experimental conditions. N_2O_5 is not formed in detectable quantities because the low NO_3 concentration limits the reaction of $NO_2 + NO_3 \rightarrow N_2O_5$. These model results explain why nitrogen oxides other than NO, NO_2 and N_2O are undetectable in our experiments.

Model parameters obtained for different O_2 concentrations for the three electron collision reactions (R37-R39) are shown in Figure 6. For each electron collision, model parameter α remains constant with oxygen concentration (Figure 6(a)). However, model parameter β decays with oxygen concentration as a power function (Figure 6(b)-(d)). Applying a least square regression analysis to these data, β is found to be inversely proportional to the mole fraction of oxygen to a different power for each electron collision reaction:

$$\text{For R37:} \quad \beta = 2.00 \times 10^{-5} \cdot x_{O_2}^{-0.817} \tag{5a}$$

$$\text{For R38:} \quad \beta = 4.00 \times 10^{-7} \cdot x_{O_2}^{-0.314} \tag{5b}$$

$$\text{For R39:} \quad \beta = 5.55 \times 10^{-7} \cdot x_{O_2}^{-0.0726} \tag{5c}$$

where x_{O_2} is the mole fraction of oxygen. All model parameters β for electron collision reactions R37-R39 are oxygen concentration dependent because the expression for the rate constant of electron collision reactions involves the effect of electron concentration, as shown in Eq. (4). However, electron concentration changes with oxygen concentration in the plasma, as observed

by Kanazawa *et al.*.[13] Figure 7(a) shows the rate constants of electron collision reactions R37-R39 (calculated from Eq. (4)) as a function of O_2 concentration at 100 W power input. The rate constant of electron collision reactions decrease with increasing oxygen concentration. Oxygen is electronegative; it has a strong electron affinity (0.45 eV).[11] The presence of O_2 as a reactant reduces the discharge current by capturing electrons and therefore reduces the electron concentration during discharge due to the electron attachment process, as observed by Sathiamoorthy *et al.*,[2] Kanazawa *et al.*[13] and Mok *et al.*,[14] which results in the decreasing values in the rate constants observed in Figure 7(a).

Figure 7(b) shows the ratio of the rate constant of electron collision reaction with oxygen to the rate constants of electron collision with nitrogen as a function of oxygen mole fraction at different power inputs. The rate constant for N_2 dissociation is approximately two orders of magnitude less than that for O_2 dissociation. McLarnon and Penetrante[17] used theoretical calculations (the Boltzmann code ELENDIF) to estimate the rate constant of electron collision reactions. When they compared the ratio of the rate constants of electron collision reactions with oxygen and nitrogen, they found similar results, which support the validity of our lumped model analysis. At a constant oxygen concentration, Figure 7(b) also shows that the rate constant ratio weakly increases with increasing power input because oxygen has a lower dissociation energy compared to nitrogen dissociation, as discussed earlier.

Substituting the expressions for β from Eq. 5(a)-(c) in Eq.(4), the expressions for the rate of electron collision reactions for R37-R39 become

$$R_{37} = 2.00 \times 10^{-5} \cdot x_{O_2}^{0.183} \cdot \sqrt{\frac{1}{\alpha P}} \cdot W^{0.75} \cdot \exp(-\frac{\alpha P}{W}) \cdot \frac{P}{RT} \tag{6a}$$

$$R_{38} = 4.00 \times 10^{-7} \cdot x_{O_2}^{-0.314} \cdot (1 - x_{O_2}) \cdot \sqrt{\frac{1}{\alpha P}} \cdot W^{0.75} \cdot \exp(-\frac{\alpha P}{W}) \cdot \frac{P}{RT} \tag{6b}$$

$$R_{39} = 5.55 \times 10^{-7} \cdot x_{O_2}^{-0.0726} \cdot (1 - x_{O_2}) \cdot \sqrt{\frac{1}{\alpha P}} \cdot W^{0.75} \cdot \exp(-\frac{\alpha P}{W}) \cdot \frac{P}{RT} \qquad (6c)$$

where R_n is the rate of reaction n, R is the gas constant, and T is gas temperature. These equations indicate that the rate of the electron-oxygen collision reaction increases with increasing oxygen concentration, while the rate of electron-nitrogen collision reactions decreases with increasing oxygen content. Figure 8(a) shows these rate trends for the three electron collision reactions as a function of O_2 concentration. Using the definition of selectivity given by Eq.3(a)-(d), selectivities for the three parallel electron collision reactions R37-R39 are shown in Figure 8(b). The selectivity of R37 increases with increasing oxygen concentration, while the selectivity of R38 and R39 decreases with increasing oxygen concentration, which is consistent with the results in Figure 8(a). The oxygen reaction (R37) selectivity is always far higher than the selectivity of nitrogen reactions (R38 and R39) over the range of oxygen concentrations examined in this work, which is consistent with the results reported by Penetrante et al.[21] They found that discharge plasma conditions with mean electron energy of less than 10 eV are optimum for the dissociation of O_2 in preference of N_2 because a significant fraction of the input power is consumed by dissociation of O_2. This suggests that most of NO would be converted into NO_2 by the reaction with O (R28) in the presence of O_2.

In addition, the similar selectivity of electron collision reactions R38 and R39 indicates that the branch ratio for $N(^4S)$ and $N(^2D)$ formation through electron collision reactions with N_2 is approximately one, which is consistent with the results reported by Cosby,[39] who found that e + $N_2 \rightarrow N(^4S) + N(^2D)$ is the dominant dissociation mechanism. In hindsight, the similar nitrogen reaction selectivities suggest that this single reaction could be used to replace both R38 and R39 to decrease the number of parameters in the model by two. Evaluation of the model

with only four parameters (α and β for each of the electron collision reactions, R37 and e + N_2 $\rightarrow$ N(^{4}S) + N(^{2}D)) confirmed that such a model is as accurate as the six parameter model.

Critical O$_2$ concentration for NO$_x$ formation and conversion

The reaction mechanism of NO$_x$ conversion in the presence of oxygen, shown in Table 4, suggests that NO is converted to N_2 and O_2 through reduction with N(^{4}S) and N(^{2}D) (R48 and R56) and is formed through oxidation with N(^{2}D) (R6). Therefore, the O_2 concentration at which the production of NO by N(^{2}D) counterbalances the reduction of NO by N(^{4}S) and N(^{2}D) is a critical value. Figure 9 shows an example of the lumped model calculation results, in which the NO$_x$ conversion, defined in Eq. (2), changes as a function of oxygen concentration for an inlet concentration of 350 ppm NO at different specific energy inputs. The same model parameters as those discussed in the previous section were used in this calculation for the three electron collision reactions R37-R39 (Figure 5). NO$_x$ conversion of zero implies that the reduction of NO to N_2 and O_2 is counterbalanced by the formation of NO, resulting in a constant total NO$_x$ concentration in the reactor. The results in Figure 9 show that the NO$_x$ conversion for all specific energy inputs converges to zero at almost the same oxygen concentration (~2.5%), which is consistent with the previous experimental observation (Figure 3(d)). At lower oxygen concentrations, NO$_x$ conversion is positive, which means that NO is being converted to N_2 and O_2 faster than it is being produced. At higher oxygen concentrations, NO$_x$ conversion is negative, which means that NO is formed through reaction R6 faster than it is decomposed. The oxygen concentration at which NO$_x$ conversion is zero is defined as the critical oxygen concentration.

Figure 9 shows that, in general, at a given specific energy input, NO$_x$ conversion initially decreases with increasing oxygen concentration and reaches a minimum negative value (i.e., when the NO$_x$ formation rate is maximum). This minimum in NO$_x$ conversion occurs because

the rate of R6 is controlled by the concentration of both O_2 and $N(^2D)$. At low oxygen concentrations, the effect of increasing oxygen concentration is dominant. However, increasing oxygen concentration causes the nitrogen concentration to decrease, which leads to a decrease of the $N(^2D)$ concentration. When the increase in oxygen concentration is unable to compensate for the decrease in $N(^2D)$ concentration (at O_2 mole fractions of about 0.13), the observed minimum in NO_x conversion occurs.

The consumption of $N(^2D)$ occurs predominantly through R6, R56 and R58. The rate of R57 is negligible because the concentration of N_2O is very low, as shown in Figure 4(c). At oxygen concentrations below the critical concentration, reactions R56 and R58 prevail, resulting in net NO conversion. However, at oxygen concentrations above the critical concentration, R6 prevails, resulting in net NO formation. The formation rate of $N(^2D)$ increases with increasing specific energy input, as shown in Eq.6(c). Therefore, at a given oxygen concentration, NO_x conversion increases with increasing specific energy input below the critical concentration, while NO_x conversion decreases (corresponding to NO_x formation) with increasing specific energy input above the critical concentration, as shown in Figure 9.

Figure 10 shows the critical oxygen concentration as a function of initial NO concentration modeled at six specific energy inputs. The critical oxygen concentration increases with initial NO concentration. Consumption of $N(^2D)$ by NO conversion through R56 increases with initial NO concentration, which results in a decrease of $N(^2D)$ consumption to form NO through R6. Therefore, higher oxygen concentrations are required to increase the reaction rate of R6 in order to counterbalance the reaction rate of R56. Figure 10 also shows that the critical concentrations for different specific energy inputs at the same initial NO concentration are approximately equal, which is consistent with the convergence point shown in Figure 9.

Conclusions

In general, oxygen reduces NO_x conversion and increases its formation in a pulsed corona discharge reactor. Ozone and nitrogen oxides other than NO, NO_2 and N_2O are not detected at the outlet of the reactor in our experiments. NO is mainly converted to NO_2 by chemical oxidation in the presence of oxygen. Initial selectivity analysis shows that three electron collision reactions are important for NO_x reactions in O_2/N_2, although subsequent analysis shows that only two are required to accurately model the system. The rate constants of these electron collision reactions, calculated for different oxygen concentrations from a kinetic model, decrease with increasing oxygen concentration. The rate constant of O_2 dissociation by electron collision reaction is almost two orders of magnitude higher than that of N_2 dissociation by electron collision because oxygen has a lower dissociation energy compared to nitrogen. A reaction mechanism proposed for NO_x conversion and formation in O_2 and N_2 plasma leads to a good agreement between the model data and experimental data. NO is converted to N_2 and O_2 through reduction reactions and is formed through an oxidation reaction in the presence of oxygen in the PCDR. The mechanism of NO formation occurs mainly by the reaction of $N(^2D)$ radicals with molecular oxygen: $N(^2D) + O_2 \rightarrow NO + O$. The critical oxygen concentration, which is defined as the oxygen concentration with zero net NO_x conversion, increases with increasing initial NO concentration.

Acknowledgments

Literature cited

1 Raether H. Electron Avalanches and Breakdown in Gases. Washington: Butterworths, 1964.

2 Sathiamoorthy G, Kalyana S, Finney WC, Clark RJ, Locke BR. Chemical Reaction Kinetics and Reactor Modeling of NOx Removal in a Pulsed Streamer Corona Discharge Reactor. *Ind. Eng. Chem. Res.* 1999; 38:1844-1855.

3 Zhou Q, Yao SC, Russell A, Boyle J. Flue gas nitrogen oxide (NOx) reduction using ammonia radical injection. *J. Air Waste Manage. Assoc.* 1992; 42:1193-1197.

4 Zhao G-B, Hu X, Argyle MD, Radosz M. N Atom Radicals and $N_2(A^3\Sigma_u^+)$ Found to be Responsible for Nitrogen Oxides Conversion in Non-thermal Nitrogen Plasma. *Ind. Eng. Chem. Res.* 2004; 43:5077-5088.

5 Zhao G-B, Hu X, Yeung MC, Plumb OA, Radosz M. Nonthermal Plasma Reactions of Dilute Nitrogen Oxide Mixtures: NOx in Nitrogen. *Ind. Eng. Chem. Res.* 2004; 43:2315-2323.

6 Penetrante BM, Hsiao MC, Merritt BT, Vogtlin GE, Wallman PH. Comparison of Electrical Discharge Techniques for Nonthermal Plasma Processing of NO in N_2. *IEEE Trans. Plasma Sci.* 1995; 23:679-687.

7 Herron JT. Modeling Studies of the Formation and Destruction of NO in Pulsed Barrier Discharges in Nitrogen and Air. *Plasma Chem. Plasma Process.* 2001; 21:581-609.

8 Yan K, Kanazawa S, Ohkubo T, Nomoto Y. Oxidation and Reduction Processes During NOx Removal with Corona-Induced Nonthermal Plasma. *Plasma Chem. Plasma Process.* 1999; 19:421-443.

9 Zhao G-B, Garikipati SVBJ, Hu X, Argyle MD, Radosz M. Effect of Reactor Configuration on NO Conversion in Non-thermal Plasma Reactors. *AIChE J.* 2004, (accepted).

10 Dinelli G, Civitano L, Rea M. Industrial Experiments on Pulse Corona Simultaneous Removal of NOx and SO_2 from Flue Gas. *IEEE Trans. Ind. Appl.* 1990; 26:535-541.

11 Miller TM. Electron Affinities. In *CRC Handbook of Chemistry and Physics*, Lide DR. Ed. CRC Press: Boca Raton, 2003; p10-147.

12 Lofthus A, Krupenie PH. The Spectrum of Molecule Nitrogen. *J. Phys. Chem. Ref. Data* 1977; 6:113-307.

13 Kanazawa S, Chang JS, Round GF, Sheng G, Ohkubo T, Nomoto Y, Adachi T. Removal of NOx from flue gas by corona discharge activated methane radical showers. *J. Electrostatics* 1997; 40 & 41:651-656.

14 Mok YS, Kim JH, Nam IS, Ham SW. Removal of NO and Formation of Byproducts in a Positive-Pulsed Corona Discharge Reactor. *Ind. Eng. Chem. Res.* 2000; 39:3938-3944.

15 Gallimberti I. Impulse corona simulation for flue gas treatment. *Pure Appl. Chem.* 1988; 60:663-674.

16 Kerr JA. Strengths of Chemical Bonds. In *CRC Handbook of Chemistry and Physics*, Lide DR. Ed. CRC Press: Boca Raton, 2003; p9-56.

17 McLarnon CR, Penetrante BM. Effect of Gas Composition on the NOx Conversion Chemistry in a Plasma. *SAE Technical Papers 982433* 1998; 1-12.

18 Tas MA, van Hardeveld R, van Veldhuizen EM. Reactions of NO in a Positive Streamer Corona Plasma. *Plasma Chem. Plasma Process.* 1997; 17:371-391.

19 Takaki K, Jani MA, Fujiwara T. Removal of Nitric Oxide in Flue Gases by Multipoint to Plane Dielectric Barrier Discharge. *IEEE Trans. Plasma Sci.* 1999; 27:1137-1145.

20 Aritoshi K, Fujiwara M, Ishida M. Production and Removal Mechanisms of Discharge NOx Treatment in N_2/O_2 Gas Mixture. *Jpn. J. Appl. Phys.* 2002; 41:3936–3942.

21 Penetrante BM, Bardsley JN, Hsiao MC. Kinetic analysis of non-thermal plasmas used for pollution control. *Jpn. J. Appl. Phys.* 1997; 36:5007-5017.

22 Gentile AC, Kushner MJ. Microstreamer dynamics during plasma remediation of NO using atmospheric pressure dielectric barrier discharges. *J. Appl. Phys.* 1996; 79:3877-3885.

23 Gentile AC, Kushner MJ. Reaction chemistry and optimization of plasma remediation of NxOy from gas streams. *J. Appl. Phys.* 1995; 78:2074-2085.

24 Kim DJ, Choi Y, Kim KS. Effects of Process Variables on NOx Conversion by Pulsed Corona Discharge Process. *Plasma Chem. Plasma Process.* 2001; 21:625-650.

25 Lowke JJ, Morrow R. Theoretical Analysis of Removal of Oxides of Sulphur and Nitrogen in Pulsed Operation of Electrostatic Precipitators. *IEEE Trans. Plasma Sci.* 1995; 23:661-671.

26 Mukkavilli S, Lee CK, Varghese K, Tavlarides LL. Modeling of the Electrostatic Corona Discharge Reactor. *IEEE Trans. Plasma Sci.* 1988; 16:652-660.

27 Orlandini I, Riedel U. Chemical kinetics of NO removal by pulsed corona discharges. *J. Phys. D: Appl. Phys.* 2000; 33:2467-2474.

28 Hu X, Nicholas J, Zhang JJ, Linjewile TM, de Filippis P, Agarwal PK. The Destruction of N_2O in a Pulsed Corona Discharge Reactor. *Fuel* 2002; 81:1259-1268.

29 Schweitzer F, Mirabel P, George C. Multiphase chemistry of N_2O_5, $ClNO_2$, and $BrNO_2$. *J. Phys. Chem. A* 1998; 102:3942-3952.

30 Vogtlin GE. Pulsed Corona Discharge for Removal of NOx from Flue Gas. In *Non-Thermal Plasma Techniques for Pollution Control-Part B: Electron Beam and Electrical Discharge*, Penetrante BM, Schultheis SE. Ed. Springer-Verlag: Berlin, Heidelberg, 1993; G34, Part B:187-198.

31 Herron JT, Green DS. Chemical Kinetics Database and Predictive Schemes for Nonthermal Humid Air Plasma Chemistry. Part II. Neutral Species Reactions. *Plasma Chem. Plasma Process.* 2001; 21:459-481.

32 Piper LG. Energy transfer studies on $N_2(X^1\Sigma_g^+,v)$ and $N_2(B^3\Pi g)$. *J. Chem. Phys.* 1992; 97: 270-275.

33 Smirnov SA. Rybkin VV, Kholodkov IV, Titov VA. Simulation of the processes of formation and dissociation of neutral particles in air plasma: kinetics of neutral components. *High Temp.* 2002; 40:323-330.

34 Piper LG. Quenching Rate Coefficients for $N_2(a'^1\Sigma_u^-)$. *J. Chem. Phys.* 1987; 87:1625-1629.

35 Marinelli WJ, Kessler WJ, Green BD, Blumberg WAM. Quenching of $N_2(a^1\Pi_g, v'=0)$ by N_2, O_2, CO, CO_2, CH_4, H_2, and Ar. *J. Chem. Phys.* 1989; 90:2167-2173.

36 Herron JT. Evaluated Chemical Kinetics Data for Reactions of $N(^2D)$, $N(^2P)$, and $N_2(A^3\Sigma_u^+)$ in the Gas Phase. *J. Phys. Chem. Ref. Data* 1999; 28:1453-1483.

37 Fernandez A, Goumri A, Fontijn A. Kinetics of the Reactions of $N(^4S)$ Atoms with O_2 and CO_2 over Wide Temperatures Ranges. *J. Phys. Chem. A.* 1998; 102:168-172.

38 Atkinson R, Baulch DL, Cox RA, Hampson JRF, Kerr JA, Troe J. Evaluated Kinetic and Photochemical Data for Atmospheric Chemistry: Supplement III. *J. Phys. Chem. Ref. Data* 1989; 18:881-1097.

39 Cosby PC. Electron-impact Dissociation of Nitrogen. *J. Chem. Phys.* 1993; 98:9544-9553.

40 Hill RD, Rahmim I, Rinker RG. Experimental Study of the Production of NO, N_2O, and O_3 in a Simulated Atmospheric Corona. *Ind. Eng. Chem. Res.* 1988; 27:1264-1269.

41 Krupenie PH. Spectrum of molecular oxygen. *J. Phys. Chem. Ref. Data* 1972; 1:423-534.

42 Mok YS, Ham SW. Conversion of NO to NO_2 in Air by a Pulsed Corona Discharge Process. *Chem. Eng. Sci.* 1998; 53:1667-1678.

43 Simek M, Babicky V, Clupek M, DeBenedictis S, Dilecce G, Sunka P. Excitation of N_2(C $^3\Pi_u$) and NO(A $^2\Sigma^+$) states in a pulsed positive corona discharge in N_2, N_2-O_2 and N_2-NO mixtures. *J. Phys. D: Appl. Phys.* 1998; 31:2591-2602.

44 Eliasson B, Kogelschatz U. Electron Impact Dissociation in Oxygen. *J. Phys. B: At. Mol. Phys.* 1986; 19:1241-1247.

45 http://gaphyor.lpgp.u-psud.fr/gaphyor.

46 http://kinetics.nist.gov/index.php.

47 Schofield K. Critically evaluated rate constants for gaseous reactions of several electronically excited species. *J. Phys. Chem. Ref. Data* 1979; 8:723-798.

48 Atkinson R, Baulch DL, Cox RA, Hampson JRF, Kerr JA, Rossi MJ, Troe J. Evaluated Kinetic and Photochemical Data for Atmospheric Chemistry: Supplement VI. *J. Phys. Chem. Ref. Data* 1997; 26:1329-1499.

49 Copeland RA, Knutsen K, Onishi ME, Yalcin T. Collisional removal of O_2 (c $^1\Sigma_u^-$, v = 9) by O_2, N_2, and He. *J. Chem. Phys.* 1996; 105:10349-10355.

50 Kossyi IA, Kostinsky AY, Matveyev AA, Silakov VP. Kinetic Scheme of the Non-equilibrium Discharge in Nitrogen-Oxygen Mixtures. *Plasma Sources Sci. Technol.* 1992; 1: 207-220.

51 Kenner RD, Ogryzlo EA. Rate constant for the deactivation of molecular oxygen($A^3\Sigma_u^+$) by molecular nitrogen. *Chem. Phys. Lett.* 1983; 103:209-212.

52 Kenner RD, Ogryzlo EA. Deactivation of oxygen ($O_2(A^3\Sigma_u^+)$) by molecular oxygen, atomic oxygen, and argon. *Int. J. Chem. Kinet.* 1980; 12:501-508.

53 Cosby PC. Electron-impact dissociation of oxygen. *J. Chem. Phys.* 1993; 98:9560-9569.

54 Barnett AJ, Marston G, Wayne RP. Kinetics and chemiluminescence in the reaction of nitrogen atoms with oxygen and ozone. *J. Chem. Soc., Faraday Trans.* 1987; 83:1453-63.

Table Captions

Table 1. Experiments at 217 kPa

Table 2. Initial selectivity of consumption of active species of nitrogen by radiation, quenching,

O$_2$ dissociation and NO$_x$ conversion

Table 3. Chemical reactions and rate constants relevant to active species of oxygen

Table 4. Chemical reactions and rate constants for NO$_x$ in N$_2$/O$_2$

Table 1. Experiments at 217 kPa

System	Flowrate (m^3/s)	Residence time (s)
659 ppm NO + N_2	1.81×10^{-4}	20.8
2.28% O_2 + 355 ppm NO + N_2	2.64×10^{-4}	14.3
4.60% O_2 + 358 ppm NO + N_2	2.54×10^{-4}	14.8
7.07% O_2 + 428 ppm NO + N_2	2.58×10^{-4}	14.8
13.6% O_2 + 437 ppm NO + N_2	2.54×10^{-4}	14.9

Table 2. Initial selectivity of consumption of active species of nitrogen by radiation, quenching, O_2 dissociation and NO_x conversion

Active species	k_I (s^{-1})	$k_q C_{N2}$ (s^{-1})	$k_d C_{O2}$ (s^{-1})	$k_r C_{NOx}$ (s^{-1})	S_I (%)	S_q (%)	S_d (%)	S_r (%)
$N_2(A^3\Sigma_u^+)$	0.526	154	2.99×10^6	4.08×10^5	~ 0	~ 0	88.0	~ 12.0
$N_2(B^3\Pi_g)$	2×10^5	1.54×10^9	2.38×10^8	1.26×10^7	~ 0	86.0	13.3	0.7
$N_2(B'^3\Sigma_u^-)$	2.60×10^4	1.54×10^9	2.38×10^8	1.26×10^7	~ 0	86.0	13.3	0.7
$N_2(a'^1\Sigma_u^-)$	43.5	9.68×10^6	3.35×10^7	1.13×10^7	~ 0	17.8	61.5	20.7
$N_2(a^1\Pi_g)$	1.80×10^4	1.12×10^9	5.13×10^8	1.13×10^7	~ 0	68.1	31.2	0.7
$N_2(W^1\Delta_u)$	6.50×10^2	5.11×10^8	[-]	1.13×10^7	~ 0	96.5	[-]	3.5
$N_2(C^3\Pi_u)$	2.73×10^7	5.11×10^8	3.58×10^8	[-]	3.0	57.0	39.9	[-]
$N_2(E^3\Sigma_g^+)$	5.26×10^3	5.11×10^8	[-]	[-]	~ 0	100	[-]	[-]
$N(^2D)$	1.07×10^{-5}	8.66×10^5	6.20×10^6	1.88×10^6	~ 0	9.7	69.3	21.0
$N(^4S)$	0	0	118	9.74×10^5	0	0	~0	100

Table 3. Chemical reactions and rate constants relevant to active species of oxygen

Chemical reaction	Rate constant*	Source	No.
$O_2(a^1\Delta_g)$ reactions			
$O_2(a^1\Delta_g) \rightarrow O_2 + h\nu$	3.70×10^{-4}	Schofield[47]	R8
$O_2(a^1\Delta_g) + N_2 \rightarrow O_2 + N_2$	8.43×10^4	Atkinson et al.[48]	R9
$O_2(a^1\Delta_g) + O_2 \rightarrow O_2 + O_2$	9.63×10^5	Atkinson et al.[48]	R10
$O_2(a^1\Delta_g) + NO \rightarrow O_2 + NO$	1.51×10^{13}	Smirnov et al.[33]	R11
$O_2(b^1\Sigma_g^+)$ reactions			
$O_2(b^1\Sigma_g^+) \rightarrow O_2 + h\nu$	9.09×10^{-2}	Schofield[47]	R12
$O_2(b^1\Sigma_g^+) + N_2 \rightarrow O_2 + N_2$	1.26×10^9	Atkinson et al.[48]	R13
$O_2(b^1\Sigma_g^+) + O_2 \rightarrow O_2 + O_2$	2.47×10^7	Atkinson et al.[48]	R14
$O_2(b^1\Sigma_g^+) + NO \rightarrow O_2 + NO$	2.41×10^{10}	Smirnov et al.[33]	R15
$O_2(c^1\Sigma_u^-)$ reactions			
$O_2(c^1\Sigma_u^-) \rightarrow O_2 + h\nu$	10^{-4}	Schofield[47]	R16
$O_2(c^1\Sigma_u^-) + N_2 \rightarrow O_2 + N_2$	1.93×10^{12}	Copeland et al.[49]	R17
$O_2(c^1\Sigma_u^-) + O_2 \rightarrow O_2 + O_2$	3.13×10^{12}	Copeland et al.[49]	R18
$O_2(C^3\Delta_u)$ reactions			
$O_2(C^3\Delta_u) \rightarrow O_2 + h\nu$	10^{-5}	Schofield[47]	R19
$O_2(C^3\Delta_u) + N_2 \rightarrow O_2 + N_2$	1.81×10^{11}	Kossyi et al.[50]	R20
$O_2(C^3\Delta_u) + O_2 \rightarrow O_2 + O_2$	1.75×10^{11}	Kossyi et al.[50]	R21
$O_2(A^3\Sigma_u^+)$ reactions			
$O_2(A^3\Sigma_u^+) \rightarrow O_2 + h\nu$	5	Schofield[47]	R22
$O_2(A^3\Sigma_u^+) + N_2 \rightarrow O_2 + N_2$	5.60×10^9	Kenner and Ogryzlo[51]	R23
$O_2(A^3\Sigma_u^+) + O_2 \rightarrow O_2 + O_2$	1.75×10^{11}	Kenner and Ogryzlo[52]	R24
$O_2(A^3\Sigma_u^+) + N_2O \rightarrow O_2 + N_2O$	2.83×10^{12}	Schofield[47]	R25

$O_2(B^3\Sigma_u^-)$ reactions

$O_2(B^3\Sigma_u^-) \rightarrow O_2 + h\nu$	2.50×10^7	Schofield[47]	R26

$O(^3P)$ reactions

$O(^3P) + O_2 \rightarrow O_3$	1.76×10^{10}	Atkinson et al.[48]	R27
$O(^3P) + NO \rightarrow NO_2$	2.45×10^{12}	Atkinson et al.[48]	R28
$O(^3P) + NO_2 \rightarrow NO_3$	2.03×10^{12}	Atkinson et al.[48]	R29

$O(^1D)$ reactions

$O(^1D) \rightarrow O_2 + h\nu$	6.76×10^{-3}	Cosby[53]	R30
$O(^1D) + N_2 \rightarrow O(^3P) + N_2$	1.57×10^{13}	Herron and Green[31]	R31
$O(^1D) + O_2 \rightarrow O(^3P) + O_2$	2.41×10^{13}	Herron and Green[31]	R32
$O(^1D) + NO \rightarrow products$	2.41×10^{13}	Herron and Green[31]	R33
$O(^1D) + NO_2 \rightarrow NO + O_2$	8.43×10^{13}	Herron and Green[31]	R34
$O(^1D) + N_2O \rightarrow NO + NO$	4.33×10^{13}	Herron and Green[31]	R35
$O(^1D) + N_2O \rightarrow N_2 + O_2$	2.65×10^{13}	Herron and Green[31]	R36

* The units of the rate constants are s^{-1} for radiation reactions and $cm^3 \cdot mol^{-1} \cdot s^{-1}$ for bimolecular reactions.

Table 4. Chemical reactions and rate constants for NO$_x$ in N$_2$/O$_2$

Chemical reaction	Rate constant (cm^3·mol^{-1}·s^{-1})	Source	No.
e + O$_2$ → O(^{3}P) + O(^{3}P) + e	$k_{37} = \dfrac{\beta_1}{[e]}\sqrt{\dfrac{1}{\alpha_1 P}}W^{0.75}\exp(-\dfrac{\alpha_1 P}{W})$	This work	R37
e + N$_2$ → N(^{4}S) + N(^{4}S) + e	$k_{38} = \dfrac{\beta_2}{[e]}\sqrt{\dfrac{1}{\alpha_2 P}}W^{0.75}\exp(-\dfrac{\alpha_2 P}{W})$	This work	R38
e + N$_2$ → N(^{2}D) + N(^{2}D) + e	$k_{39} = \dfrac{\beta_3}{[e]}\sqrt{\dfrac{1}{\alpha_3 P}}W^{0.75}\exp(-\dfrac{\alpha_3 P}{W})$	This work	R39
N(^{4}S) + NO → N$_2$ + O(^{3}P)	1.87×10^{13}	Atkinson et al.[38]	R48
N(^{4}S) + NO$_2$ → N$_2$O + O(^{3}P)	1.81×10^{12}	Atkinson et al.[38]	R49
N(^{4}S) + NO$_2$ → N$_2$ + O$_2$	4.21×10^{11}	Kossyi et al.[50]	R50
N(^{4}S) + NO$_2$ → N$_2$ + 2O(^{3}P)	5.48×10^{11}	Kossyi et al.[50]	R51
N(^{4}S) + NO$_2$ → 2NO	1.38×10^{12}	Kossyi et al.[50]	R52
N(^{4}S) + N(^{4}S) + N$_2$ → N$_2$ + N$_2$	1.59×10^{15} [N$_2$]	Kossyi et al. [50]	R53
N(^{4}S) + O(^{3}P) + N$_2$ → NO + N$_2$	3.68×10^{15} [N$_2$]	Kossyi et al. [50]	R54
N(^{4}S) + O$_2$ → NO + O(^{3}P)	5.91×10^7	Fernandez et al.[37]	R7
N(^{4}S) + O$_3$ → NO + O$_2$	6.02×10^7	Barnett et al.[54]	R55
N(^{2}D) + O$_2$ → NO + O(^{3}P)	3.13×10^{12}	Herron[36]	R6
N(^{2}D) + NO → N$_2$ + O(^{3}P)	3.61×10^{13}	Herron[36]	R56
N(^{2}D) + N$_2$O → NO + N$_2$	1.32×10^{12}	Herron[36]	R57
N(^{2}D) + N$_2$ → N + N$_2$	1.02×10^{10}	Herron[36]	R58
O(^{3}P) + O$_2$ + N$_2$ → O$_3$ + N$_2$	2.03×10^{14}[N$_2$]	Atkinson et al.[48]	R59
O(^{3}P) + O$_2$ + O$_2$ → O$_3$ + O$_2$	2.17×10^{14}[O$_2$]	Atkinson et al.[48]	R60
O(^{3}P) + O$_3$ → O$_2$ + O$_2$	4.82×10^9	Atkinson et al.[48]	R61
O(^{3}P) + NO → NO$_2$	2.45×10^{12}	Atkinson et al.[48]	R28
O(^{3}P) + NO$_2$ → NO$_3$	2.03×10^{12}	Atkinson et al.[48]	R29
O(^{3}P) + NO$_2$ → NO + O(^{3}P)	5.85×10^{12}	Atkinson et al.[48]	R62
O(^{3}P) + NO$_3$ → NO$_2$ + O$_2$	1.02×10^{13}	Atkinson et al.[48]	R63
O(^{3}P) + O(^{3}P) + N$_2$ → O$_2$ + N$_2$	1.10×10^{15}[N$_2$]	Kossyi et al.[50]	R64
NO + O$_3$ → NO$_2$ + O$_2$	1.08×10^{10}	Atkinson et al.[48]	R65
NO + NO$_3$ → NO$_2$ + NO$_2$	1.57×10^{13}	Atkinson et al.[48]	R66
NO + NO + O$_2$ → NO$_2$ + NO$_2$	7.25×10^9[O$_2$]	Atkinson et al.[48]	R67
NO$_2$ + O$_3$ → NO$_3$ + O$_2$	2.11×10^7	Atkinson et al.[48]	R68

Figure Captions

Figure 1. Experimental set up
(1) gas cylinder, NO + N_2; (2) gas cylinder, O_2 in N_2; (3) valve; (4) rotameter; (5) pressure gague; (6) pulsed corona discharge reactor; (7) gas bomb; (8) gas chromatograph

Figure 2. FTIR spectra at 200 Hz showing the product distribution; (a) 659 ppm NO + N_2, (b) 4.60% O2 + 358 ppm NO + N_2

Figure 3. Experimental results
(a) NO evolution with specific energy input; (b) NO_2 evolution with specific energy input; (c) N_2O evolution with specific energy input; (d) NOx conversion with specific energy input.
　　■: 659 ppm NO + N_2
　　○: 2.28% O_2 + 355 ppm NO + N_2; △: 4.60% O_2 + 358 ppm NO + N_2
　　◇: 7.07% O_2 + 428 ppm NO + N_2; ✕: 13.6% O_2 + 437 ppm NO + N_2

Figure 4. Experimental data and correlated data for varying oxygen content.
　　(a) 2.28% O_2 + 355 ppm NO + N_2, (b) 4.60% O_2 + 358 ppm NO + N_2,
　　(c) 7.07% O_2 + 428 ppm NO + N_2, (d) 13.6% O_2 + 437 ppm NO + N_2
　　Experimental data: ■ (NO), ● (NO_2), ▲ (N_2O);
　　Calculated data: —— (NO), – – – (NO_2), – · – (N_2O)

Figure 5. Ozone conversion through reaction R65 as a function of residence time assuming 50 ppm NO in the gas.

Figure 6. Model parameters as a function of O_2 concentration
Model parameter α for electron collision reactions (a); Model parameter β for electron collision reaction R37 (b), R38 (c), R39 (d). (■) R37, (●) R38, (▲) R39, (——) regression results

Figure 7. Rate constants of electron collision reactions R37-R39 as a function of O_2 concentration at 100 W power input (a); Ratio of rate constant of electron collision reaction with O_2 and N_2 as a function of O_2 concentration at different power inputs (b)

Figure 8. Rates of electron collision reactions R37-R39 as a function of O_2 concentration at 100 W power input (a); Selectivity of electron collision reactions R37-R39 as a function of O_2 concentration at 100 W power input (b)

Figure 9. NO_x conversion as a function of O_2 concentration for inlet concentration of 350 ppm NO at different specific energy input

Figure 10. Critical O_2 concentration as a function of NO concentration at different specific energy input
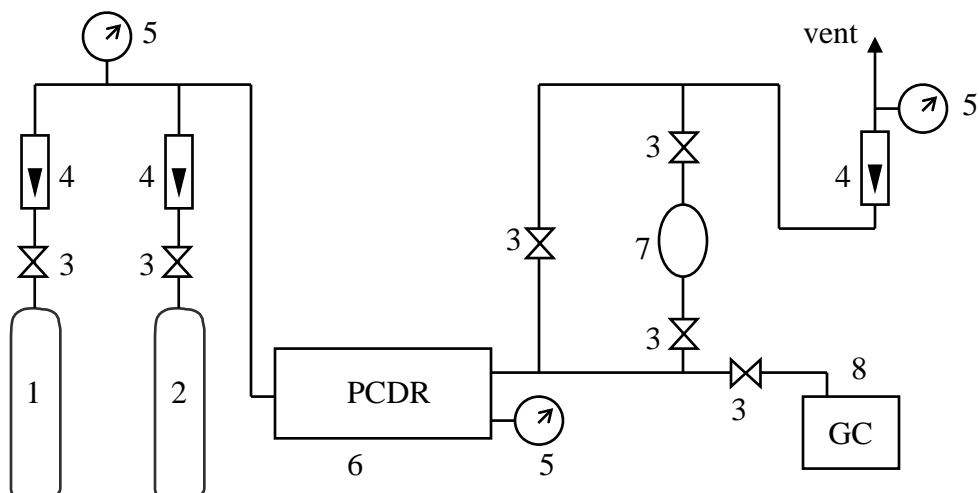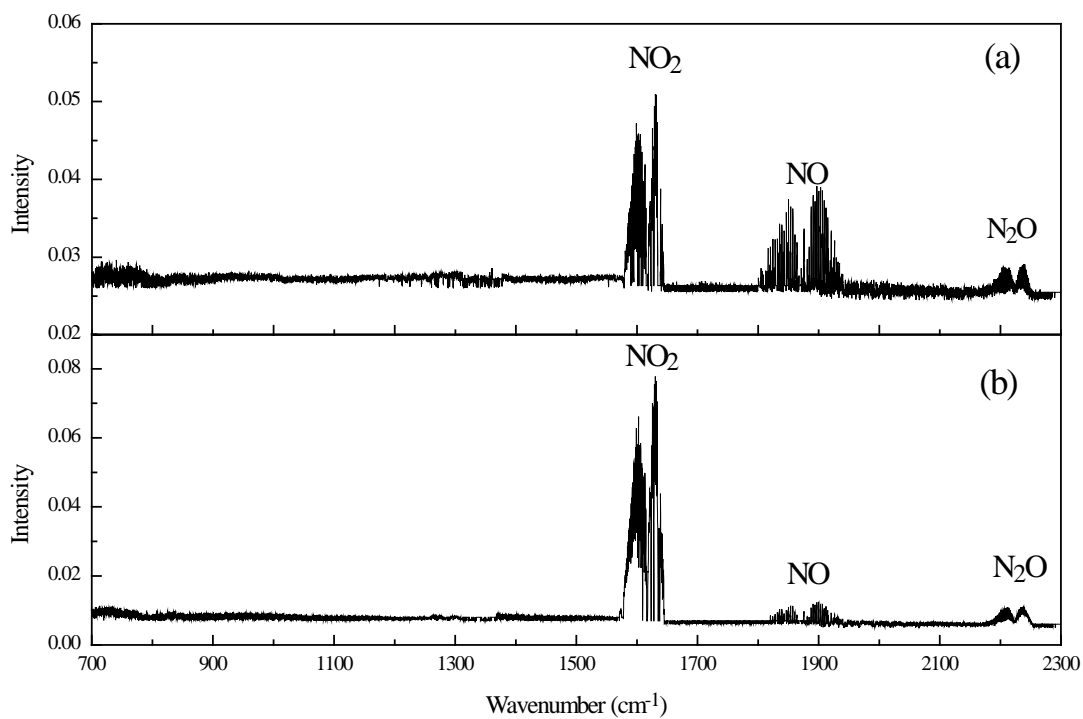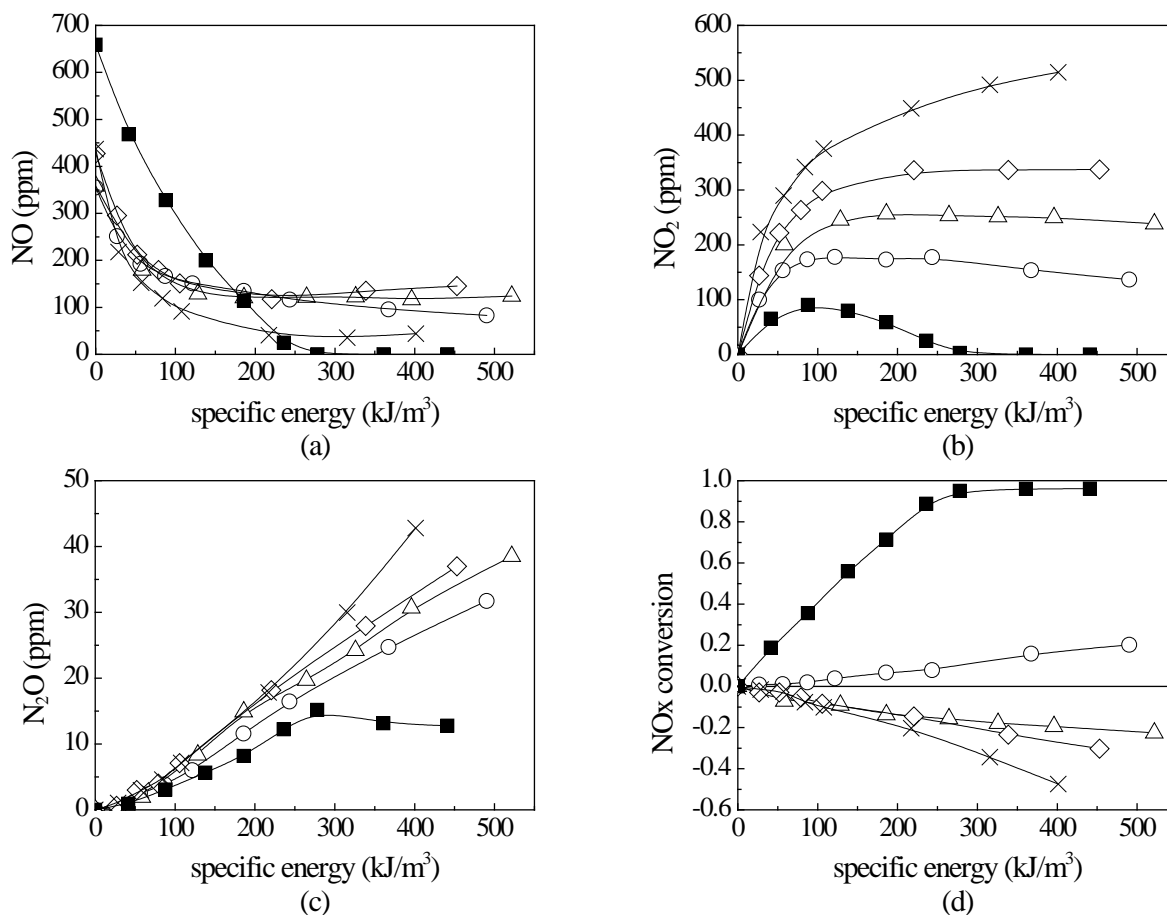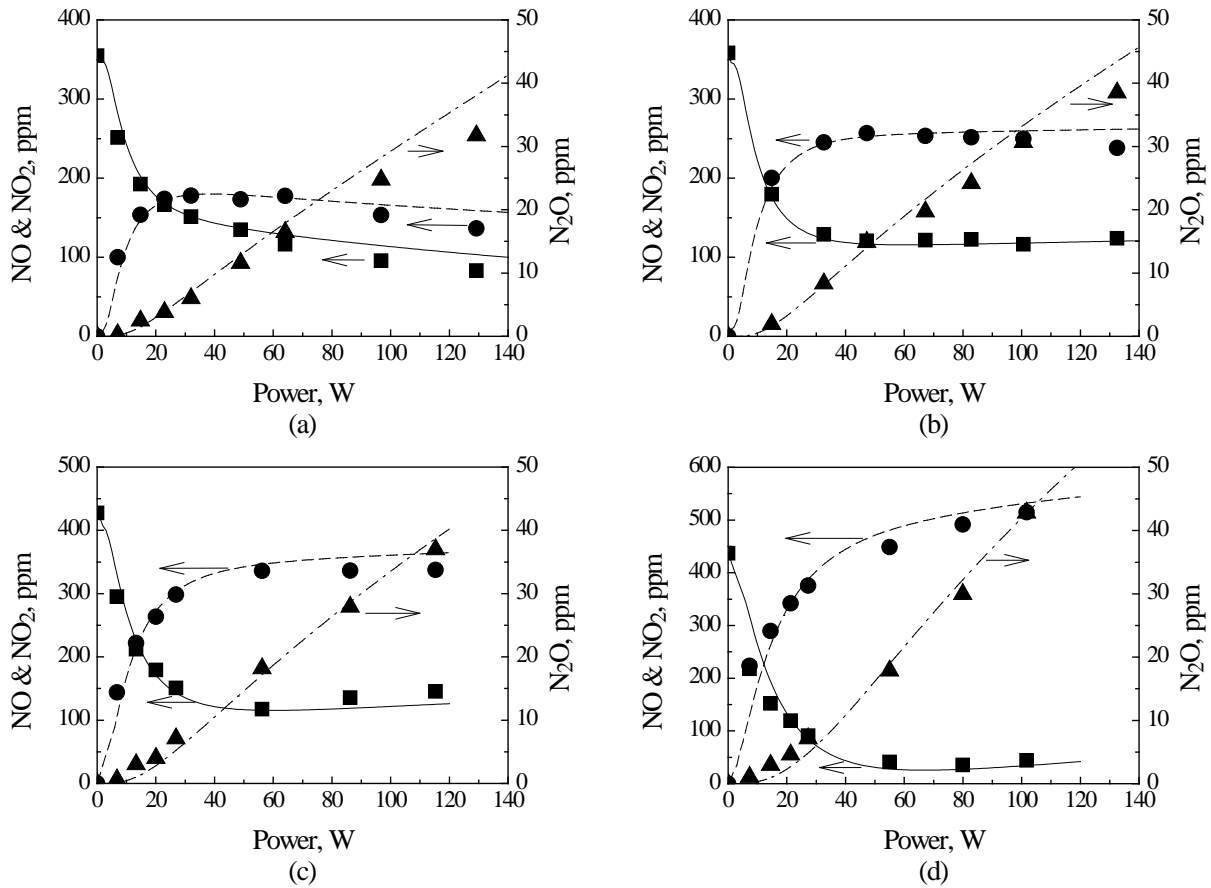
Figure 1. Experimental set up
(1) gas cylinder, NO + N_2; (2) gas cylinder, O_2 in N_2; (3) valve; (4) rotameter; (5) pressure gauge; (6) pulsed corona discharge reactor; (7) gas bomb; (8) gas chromatograph

Figure 2. FTIR spectra at 200 Hz showing the product distribution; (a) 659 ppm NO + N_2, (b) 4.60% O_2 + 358 ppm NO + N_2

Figure 3. Experimental results

(a) NO evolution with specific energy input; (b) NO_2 evolution with specific energy input; (c) N_2O evolution with specific energy input; (d) NOx conversion with specific energy input.

■: 659 ppm NO + N_2

○: 2.28% O_2 + 355 ppm NO + N_2; △: 4.60% O_2 + 358 ppm NO + N_2

◇: 7.07% O_2 + 428 ppm NO + N_2; ×: 13.6% O_2 + 437 ppm NO + N_2

Figure 4. Experimental data and correlated data for varying oxygen content.
(a) 2.28% O_2 + 355 ppm NO + N_2, (b) 4.60% O_2 + 358 ppm NO + N_2,
(c) 7.07% O_2 + 428 ppm NO + N_2, (d) 13.6% O_2 + 437 ppm NO + N_2
Experimental data: ■ (NO), ● (NO_2), ▲ (N_2O);
Calculated data: — (NO), – – – (NO_2), – · – (N_2O)

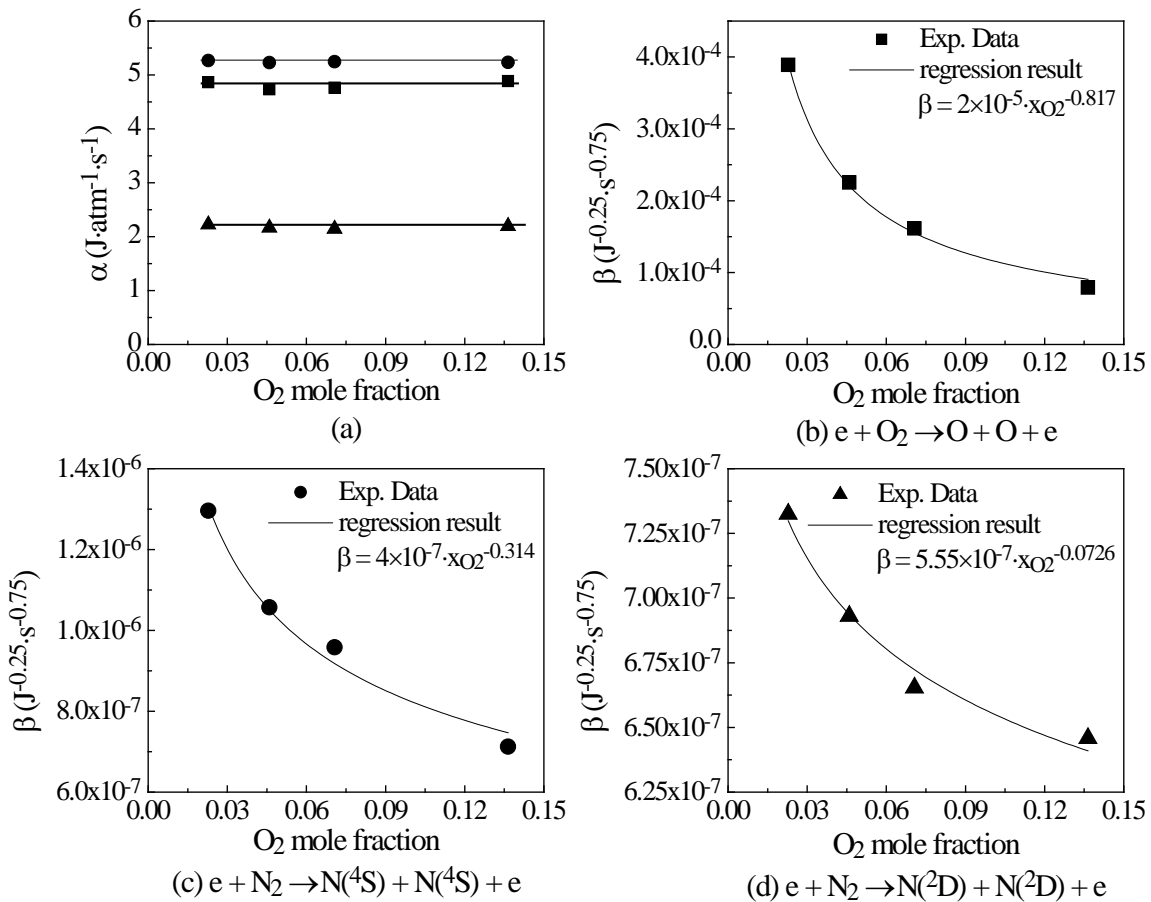**Figure 5.** Ozone conversion through reaction R65 as a function of residence time assuming 50 ppm NO in the gas.

(a)

(b) $e + O_2 \rightarrow O + O + e$

(c) $e + N_2 \rightarrow N(^4S) + N(^4S) + e$

(d) $e + N_2 \rightarrow N(^2D) + N(^2D) + e$

Figure 6. Model parameters as a function of O_2 concentration
Model parameter α for electron collision reactions (a); Model parameter β for electron collision reaction R37 (b), R38 (c), R39 (d). (■) R37, (●) R38, (▲) R39, (—) regression results

Figure 7. Rate constants of electron collision reactions R37-R39 as a function of O_2 concentration at 100 W power input (a); Ratio of rate constant of electron collision reaction with O_2 and N_2 as a function of O_2 concentration at different power inputs (b)
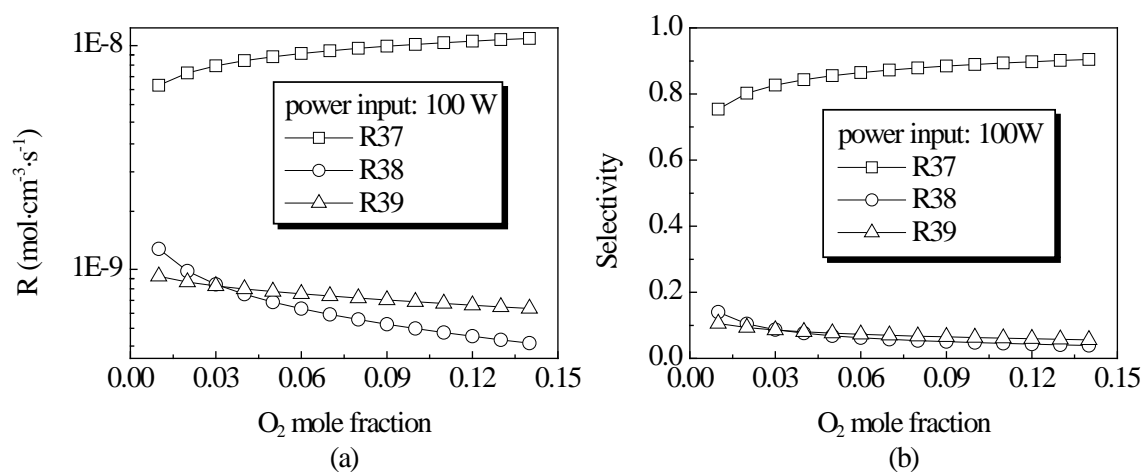

Figure 8. Rates of electron collision reactions R37-R39 as a function of O_2 concentration at 100 W power input (a); Selectivity of electron collision reactions R37-R39 as a function of O_2 concentration at 100 W power input (b)
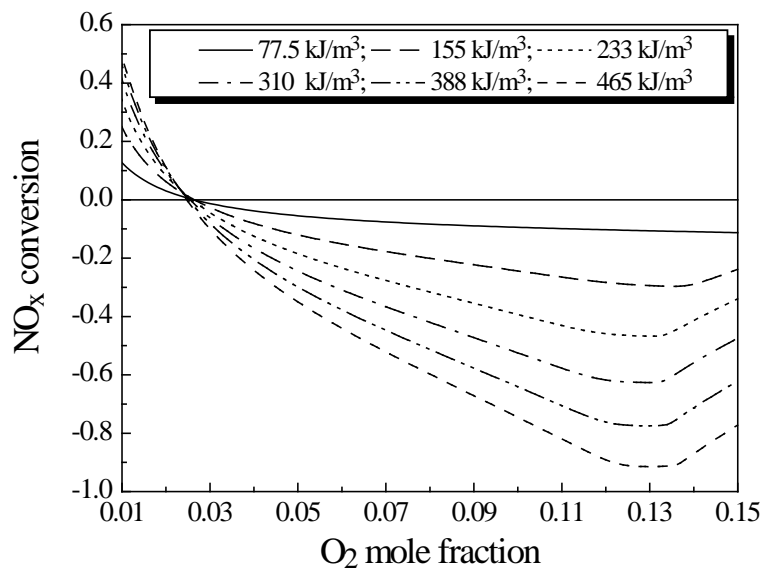
Figure 9. NO$_x$ conversion as a function of O$_2$ concentration for inlet concentration of 350 ppm NO at different specific energy input
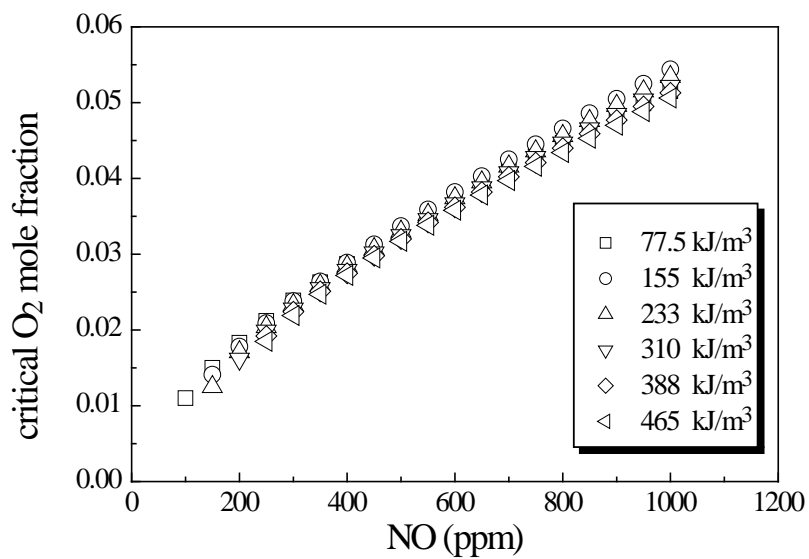

Figure 10. Critical O$_2$ concentration as a function of NO concentration at different specific energy input